Electronic and atomic structure of metal-HfO_2 interfaces

K. Y. Tse, D. Liu, and J. Robertson
Engineering Department, Cambridge University, Cambridge CB2 1PZ, United Kingdom
(Received 7 August 2009; revised manuscript received 3 November 2009; published 15 January 2010)

The interface geometry and interface barrier heights have been calculated for different interface stoichiometries and a wide range of metals on cubic HfO_2. The stable interface geometries for each stoichiometry have fourfold coordinated oxygen. Polar O rich, polar Hf rich, and various nonpolar (100), (110), and (111) interfaces are studied. The barrier heights or valence-band offsets depend strongly on the metal work function, consistent with a Schottky barrier pinning factor S of about 0.92. There is a large interface dipole for O-rich interfaces, which reduces their barrier heights by about 0.9 eV below those of the nonpolar interfaces. This offset shift is consistent with that occurring at other systems when scaled with the electronic dielectric constant. Overall, the results show little intrinsic Schottky barrier pinning by metal-induced gap states. The experimentally observed pinning in device studies after high temperature annealing is due to an extrinsic mechanism such as band bending due to charged oxygen vacancies.

DOI: 10.1103/PhysRevB.81.035325 PACS number(s): 73.30.+y, 85.30.Tv, 73.40.Qv, 61.43.Bn

I. INTRODUCTION

Metal-oxide interfaces are important for many applications such as catalysis, oxidation resistant metals, vacuum seals, thermal barrier coatings, and recently in microelectronics. The continued scaling of complementary metal oxide semiconductor (CMOS) field effect transistors (FETs) has required the replacement of the SiO_2 gate oxide by a high dielectric constant (K) oxide such as HfO_2, and the replacement of the polysilicon gate by metal gates.[1–5]

An FET works by applying a voltage to the metal gate electrode to shift the surface potential of the channel semiconductor across its band gap. If this shift is reduced in devices with high K gate oxides, for example by the presence of interface gap states, then the FET is degraded. The application of a gate potential is equivalent to changing the work function of the gate metal, and thus to a Schottky barrier. Thus, understanding the Schottky barrier performance of new materials is central to obtaining good devices from them.

The gate metals must have an effective work function with respect to the Si conduction or valence-band edges, of either 4.05 or 5.15 eV, for nFETs or pFETs, respectively.[3,6,7] This has been hindered by the presence of Fermi level pinning[7] and it has required a considerable technical effort to solve.[8–10] It appeared for some time that Fermi level pinning would prevent the implementation of metal gates because they did not seem to be able to scan the full range of effective work functions needed.[11,12] FETs using HfO_2 and metal gates are now available commercially from some manufacturers.[9]

One of the problems has been to determine experimentally[8,11,12] and theoretically[13–19] whether the band alignment or Schottky barrier height (SBH) at the metal—oxide interfaces was determined by intrinsic or extrinsic factors, that is by the bond dipoles at the interface,[14–17] or by extrinsic effects such as defect states in the oxide.[18,19]

Experimentally, the SBH of a metal-oxide interface ϕ_n will depend on the metal work function Φ_M, the oxide's electron affinity χ_s, and an oxide reference energy (measured from the vacuum level) Φ_S as

$$\phi_n = S(\Phi_M - \Phi_S) + (\Phi_S - \chi_s), \quad (1)$$

where the oxide is treated as a semiconductor. Here, S is an empirical Schottky pinning factor S which varies between the limits 0 and 1; 0 for strong pinning (the Bardeen limit) and 1 for weak pinning (Schottky limit).[20]

The metal-induced gap state (MIGS) model gives a simple picture of what determines Schottky barrier heights at metal-oxide interfaces.[5,21–24] However, it is too simple. It assumes that the barrier heights are determined only by the density and extent of the MIG states themselves, but not on the local atomic geometry and stoichiometry of the interface. This is useful as an initial estimate, but it is too severe an approximation. It is well known that the barrier heights and band offsets in other defect-free systems such as GaAs include a dipole layer term, which varies with stoichiometry.[25–32] Therefore we study this term here, by carrying out explicit calculations on a series of metal—HfO_2 interfaces of different stoichiometry and geometry/orientation.

This problem can also be considered in the broader terms of metal-oxide interfaces. Metal-oxide (ceramic) interfaces are important for many applications such as the catalyst-support interaction,[33–37] oxidation resistant metals, vacuum seals, and thermal barrier coatings. The early calculations were based on simple models such as the image charge model.[38–41] These were then extended to full atomic calculations, but using fixed atomic positions.[42,43] Finally, more recently, calculations have been carried out on fully relaxed structures.[44–56]

The calculations have shown how the binding at such interfaces is strongly ionic for metal monolayers over oxides, while thick metal layers bind by the polarization or induced charge.[46] The early calculations focused on lattice-matched systems such as Ag:MgO. More recently, calculations have treated the technologically more relevant oxides Al_2O_3 or ZrO_2.[47–50,54] Our calculations mark a case where we have studied a wide range of metals of very different work function on a specific oxide, to understand chemical trends in both bonding and in Schottky barrier heights.

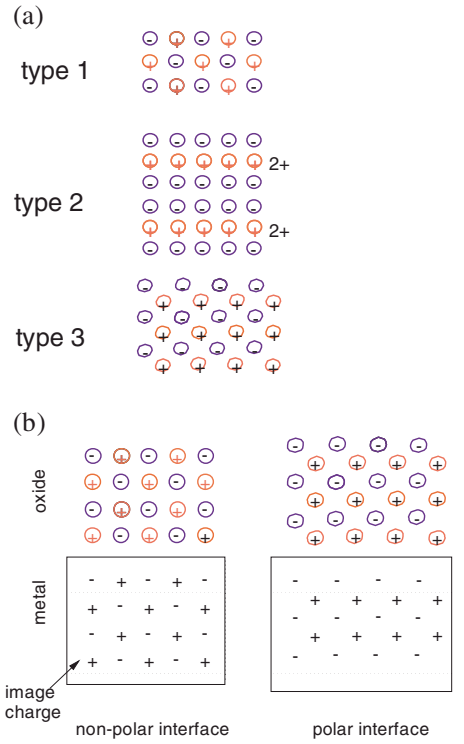

FIG. 1. (Color online) (a) Schematic of the three different types of ionic solid surface. (b) Interfaces of ionic solid with a metal showing image charge for nonpolar and polar interfaces.

Note that while HfO_2 is a transition metal oxide, it is a simple, closed shell, wide-gap oxide just like MgO, but with empty Hf *d* states rather than Mg *s* states as a conduction band. It is not correlated oxide system such as V_2O_3, or manganites, etc.

II. METHOD

To obtain the intrinsic variation of the Schottky barrier heights of metal-HfO_2 interfaces, we calculated the barrier heights for epitaxial interfaces of various metals on cubic HfO_2. This calculation requires the metal to be lattice matched to HfO_2. In practice, only Ni and Co are lattice matched to cubic HfO_2 to within 2%. For the other metals, we can force their lattices to match along the interface and allow them to relax perpendicular to the interface. In addition, all internal atomic coordinates are allowed to relax. To test the widest range of metals, we take all the metals to be FCC, even if this is not their most stable phase. This is possible because the cohesive energy of metals depends to first order on atomic volume and only second order on their structure.[57]

We use supercells containing typically five units of oxide and seven cells of metal, two interfaces, and no vacuum layer, giving a total of 31 atoms per supercell. Although the monoclinic phase of HfO_2 is slightly more stable than the cubic phase by 0.2 eV per unit, the cubic HfO_2 lattice is used for simplicity, and is maintained by imposing mirror symmetry on the supercell.

The calculations were carried out using the plane wave, total energy pseudopotential code CASTEP.[58] The electron-ion interactions are described by ultrasoft pseudopotentials, with a plane-wave basis set and kinetic energy cutoff of 380 eV. The exchange-correlation energy is given by the generalized gradient approximation (GGA). Geometries are optimized to give energy differences below 1 meV/atom and forces below 0.01 eV/Å. A Monkhorst-Pack *k*-space grid of $4\times4\times1$ to $8\times8\times1$ and $2\times4\times1$ to $4\times8\times1$ was used to converge the cell geometries of (001) and (011) cells, respectively.

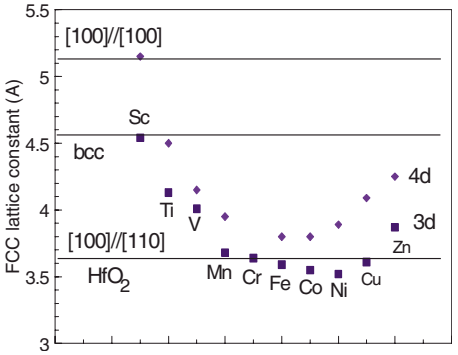

FIG. 2. (Color online) Lattice constants of 3*d* and 4*d* transition metals in their fcc phase, compared to the lattice constant of HfO_2, its 45° rotated lattice shown as [100]‖[110], and for bcc phases of the metals.

The band offsets are found by calculating the shift of the valence-band edges in the local band density of states (DOS) at atomic sites well away from the interfaces. This gives results equivalent to the electrostatic potential method. The GGA under estimates the oxide band gap, which affects the offset values. We correct the GGA valence-band offset by lowering the oxide valence band by 1.23 eV, based on the GW correction for ZrO_2,[59,60] which has a similar band gap to HfO_2.

III. RESULTS

A. Polar and nonpolar interfaces

Polar solids such as oxides can have three types of surfaces against a vacuum, as noted by Tasker[61] and Noguera,[62] Fig. 1(a). A type-1 surface is nonpolar, and gives zero electric field well away from the surface. A type-2 surface looks polar at the surface, but is actually built from nonpolar multilayer units. Overall, a type-2 surface does not create an electric field well away from the surface. Third, a type-3 surface is terminated by an excess of positive or negative ions and does create an electric field at the surface, and results in divergent potential at infinity. A type-3 surface is unstable in a vacuum due to this singularity. A similar situation for III-V semiconductors was discussed by Harrison *et al.*[63]

If these surfaces now form *interfaces* with a metal, the metal screens the electric field of a polar surface, by creating an image charge of opposite sign in the metal. This allows all three types of interface to exist in contact with a metal, including the polar type-3. The image charge for these cases is shown schematically in Fig. 1(b).

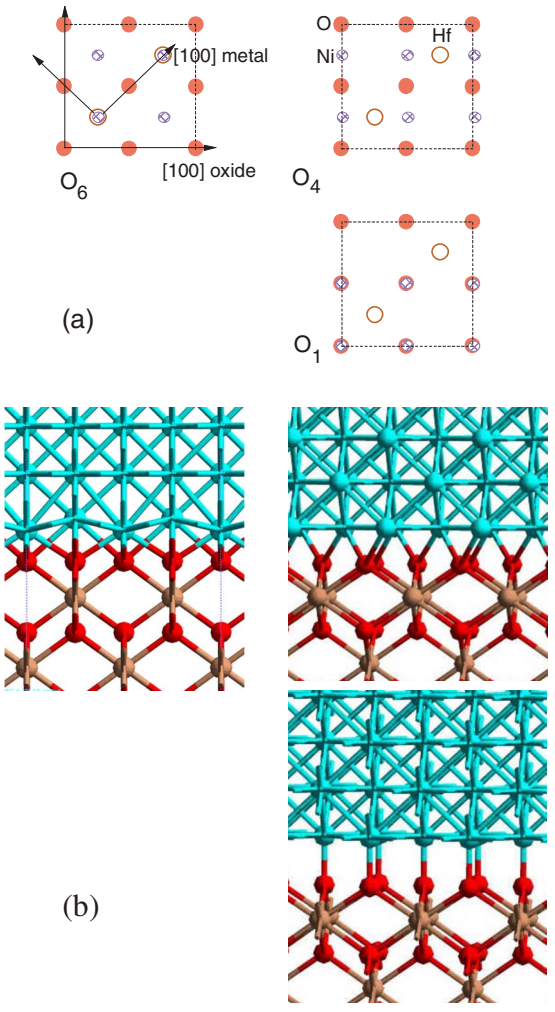

FIG. 3. (Color online) Plan view and side view of O_6, O_4 and O_1 terminated (100) metal-HfO_2 interfaces. The subscripts denote the coordination of the terminal atoms. Oxygen=red, Hf=brown, Ni=cyan.

For the cubic HfO_2 lattice, the simplest type-1 nonpolar face is (110). (111) is a type-2 nonpolar face. The (100) face is a type-3 polar interface, which can be either O terminated or Hf terminated.[64] A nonpolar (100) face can be made by taking the O-terminated interface by removing half of the oxygen in the interface layer. Figure 3 summarizes these interfaces for Ni on HfO_2.

Peressi *et al.*[30] noted that the band offset at nonpolar interfaces does not depend on the atomic configuration, whereas the band offset at polar interfaces does depend on the atomic configuration. This is because there is an additional interface dipole at the polar interface between the excess ions and its image charge in the metal.

B. Interface structures

The interface electronic structures were calculated using the supercell method. The lattice constant of the cubic HfO_2 (a=5.12 Å) is 1.4 times greater than the lattice constant of fcc Ni (a=3.52 Å), Fig. 2 Figure 3(a) shows that lattice matching is possible on their (100) faces if we rotate the Ni lattice by 45° with respect to the HfO_2, so that $a' = a/\sqrt{2}$. The interface geometries are similar to those of Si:HfO_2 (Refs. 59 and 64).

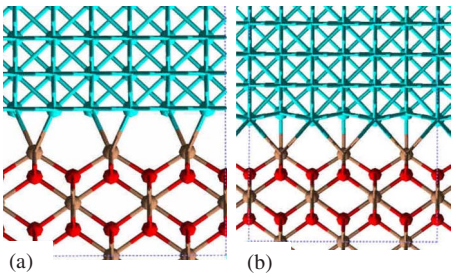

FIG. 4. (Color online) Side view of Hf_4 and Hf_6 terminated (100) metal-HfO_2 interfaces. The subscripts denote the coordination of the terminal atoms. Oxygen=red, Hf=brown, Ni=cyan.

Consider first the O-terminated (100) interface. For each interface type, we must first find the stable geometry, with respect to lateral shifts of the metal and oxide sublattices. This is equivalent to determining the coordinations of the interface oxygen ions. Figure 3(b) show three alternative configurations of the O-terminated (100) HfO_2:Ni interface, with the terminal oxygen being four, two, and onefold coordinated by Ni, or six, four, and threefold coordinated by Ni plus Hf. Figure 3(a) shows the projections onto (001). For the sixfold coordinated O_6 interface, the terminal O atom lies in the hollow above four Ni atoms and is bonded to two Hf ions in the HfO_2, Fig. 3(b). The subscripts denote the coordinations of the terminal site. If the Ni lattice is displaced by (1/4,0,0)a on HfO_2, as in Fig. 3(a), the O atom lies between two Ni atoms, and is bonded to two Ni and two Hf atoms. The site is fourfold coordinated but it is not tetrahedral.

In the last case, the Ni lattice is displaced a further (0,1/4,0)a so the O atom lies above each Ni atom. It is bonded to one Ni and two Hf atoms. The relative stability of these interfaces is calculated and a comparison finds that the O_4 case is more stable by 1.88 eV per interface cell for Ni. Beltran *et al.*[54] found a similar result. The O_4 interface is calculated to be the most stable because this coordination is compatible with the ionic radius of oxygen.

A Hf-rich interface can be formed by removing all of the interfacial oxygen. There are two likely configurations for Hf-rich, Hf_6, and Hf_8, where the terminal Hf ion is bonded to four oxygen and two or four Ni atoms, as in Fig. 4. The Hf_6 is found to be more stable than Hf_8 (Table I).

We also allowed for rumpling of the interfacial atoms at polar interfaces. The supercell symmetry was relaxed so that up-down distortions were allowed at metal and O-terminated interfaces. However, in both cases, the geometry converged to the nonrumpled geometry. Thus, the predominant form of screening of the polar interface was by image charge in the adjacent metal.

We now consider nonpolar interfaces. A nonpolar (100) can be constructed from the O-terminated (100) interface by removing half of the oxygen, as shown in Fig. 5(b). The other simple nonpolar interface is (110). Note that lattice matching is also possible on this face because the 45° rotation is possible in two directions. There are three likely interface configurations, two with fivefold oxygen and one

TABLE I. Comparison of interface energies of different configuration. The subscripts denote the coordination of the terminal atoms.

(100) O-rich	O4	O6	
Ni	0.0	1.88	
(100) Hf rich	Hf6	Hf8	
Ni	0	0.4	
(110) nonpolar	O4	O5	O5′
Ni	0	2.17	0.89
Al	0	0.99	1.43
(100) large	O4 tetrahedral	O4 planar	
La	0	1.79	
(110) large	O4 tetrahedral	O4 nontet	
La	0	1.17	
(100) O-rich bcc	O4 tetrahedral	O4 planar	O3
V	0	1.17	1.19
(110) nonpolar bcc	O4 A	O4 B	O4 C
V	0	0.24	0.27

with a fourfold oxygen site. The fourfold oxygen site is again found to be the more stable, and it is shown in Fig. 5(d). The interfacial oxygens are bonded to three Hf's and one Ni. This interface contains both O-Ni and Hf-Ni bonds. The interfacial Hf's are bonded to nine atoms, seven oxygen, and two Ni's.

The (111) is also a possible nonpolar face. We noted that lattice matching for the (100) interface is possible by a 45° rotation of the Ni lattice with respect to HfO_2. This is also possible for the (110) interface. However, it is not possible to rotate around three axes at once, so this type of matching for the (111) face is not possible. Christensen and Carter[65] did create commensurate (111) interfaces by taking cells with large periodicity along the interface plane, but this then requires overly large supercells. Instead, we constructed a quasi (111) interface by asymmetrically compressing (100) Ni to fit onto a rectangular (111) face, as shown in Fig. 5(e). This is a nonpolar interface. We thus have three nonpolar interfaces of different atomic densities. The most stable configurations of the various orientations are summarized in Fig. 5.

A few metals such as La, Y, and Sc have such a large atomic size that they cannot be realistically forced to match with HfO_2 in these structures. They can instead be matched in an FCC structure with a 1:1 epitaxy on (100) that is without the 45° rotation. There are a number of possible configurations for O-rich (100) interfaces, including two for O_4 terminations, with planar or tetrahedral oxygen. The tetrahedral O_4 interface is found to be the most stable, as in Fig. 6(a). A nonpolar version of this interface can be made by removing half of the oxygen, Fig. 6(b). A Hf-terminated interface is made by removing all interfacial oxygen and is shown in Fig. 6(c).

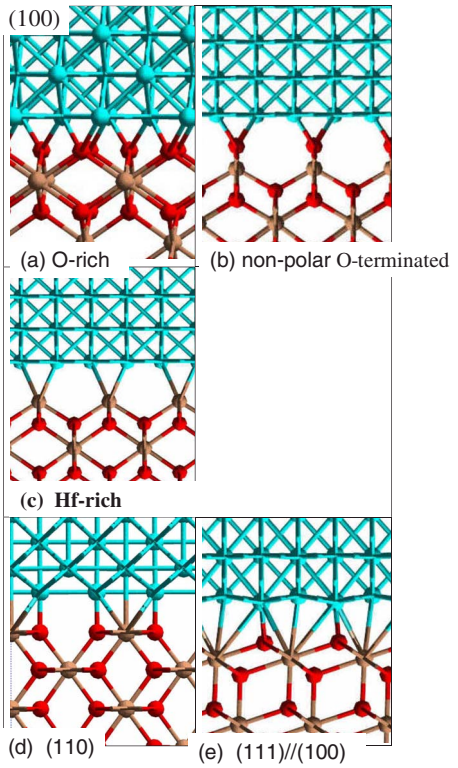

FIG. 5. (Color online) (a) O-terminated (100). (b) nonpolar (100), (c) Hf-terminated (100), (d) nonpolar (110) and (e) nonpolar (111) on (100) interfaces of fcc metals on cubic HfO_2. Oxygen =red, Hf=brown, Ni=cyan.

Figure 6(f) shows a nonpolar (110) interface for these metals. There are again a number of possibilities. The most stable is remarkable because it has only La-O and Hf-O bonds, despite being nonpolar. Figures 5(d) and 5(e) shows

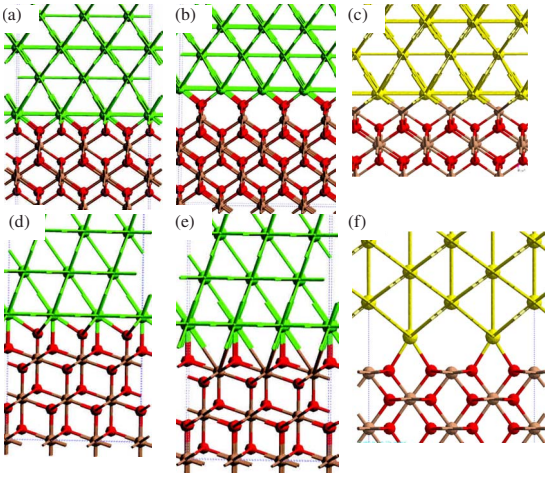

FIG. 6. (Color online) Side views of large cell interfaces with HfO_2. (a) O-terminated (100), (b) stoichiometric (100), (c) La-terminated (100). (d) O-rich (111). (e) Nonpolar (111). (f) nonpolar (110). Oxygen=red, Hf=brown, La=green or yellow.

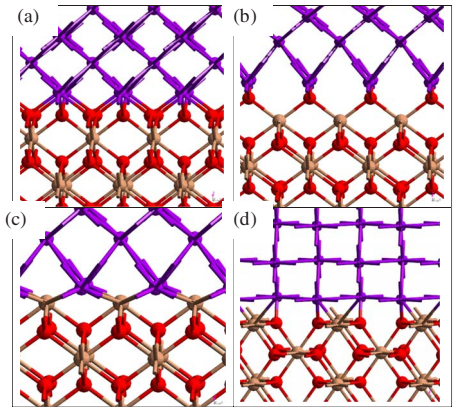

FIG. 7. (Color online) Interfaces of a bcc metal on cubic HfO_2. (a) O-terminated (100). (b) stoichiometric (100). (c) Hf-terminated (100). (d) nonpolar (110) O_4. Subscripts denote the coordination of the terminal atoms. Oxygen=red, Hf=brown, Ti=purple.

the most stable (111) O-terminated interfaces for both O rich and nonpolar cases. Again they have fourfold coordinated oxygen.

We have been able to model all metals in an fcc structure using one or other of these interfaces. However, in order to cover metals of intermediate atomic radius, larger than Ni but smaller than La, we also considered their bcc phases as in Fig. 7. The (100) face of a bcc metal is able to match to (100) face of cubic HfO_2 if the cell is rotated by 45°. The most stable configurations for O rich, nonpolar, and Hf-rich (100) interfaces are shown in Figs. 7(a)–7(c), respectively. Figure 7(d) shows the nonpolar (110) interface. Again, for O-rich interfaces, the fourfold coordinated, tetrahedral O site is the most stable, because it is compatible with oxygen's ion radius. The important difference between the interfaces of fcc and bcc metals is that the surface density of metal atoms is half that for bcc.

C. Interfacial energies

For an interface of general stoichiometry, the interface formation energy E_{int} is defined as

$$E_{int} = E_{Total} - [n\ E_{HfO_2} + m\ E_M + l\ \mu_0]/2q \qquad (2)$$

where E_{Total} is the total energy of the supercell, 2 is the two interfaces per supercell, q is the number of interface metal atoms per face (for fcc), n is the number of HfO_2 units per cell, m is the number of metal atoms in the metal layer per cell, l is the number of excess oxygen atoms not in an HfO_2 unit. E_{HfO_2} is the energy of a strained HfO_2 cell per formula unit, E_M is the energy of strained metal cell per atom and μ_0 is the chemical potential of oxygen as O_2. The O chemical potential is referred to that of oxygen in the O_2 molecule which is taken as zero. Note that we calculate the reference total energies E_M and E_{HfO2} for the strained cell in each case.

For each metal, we have plotted the interface energy of the various interfaces against μ_0, as in Fig. 8 Figure 8 shows this for Ni, which is an electronegative, high work function metal. The O chemical potential varies between μ=0 eV corresponding to the chemical potential of O_2, and −5.8 eV

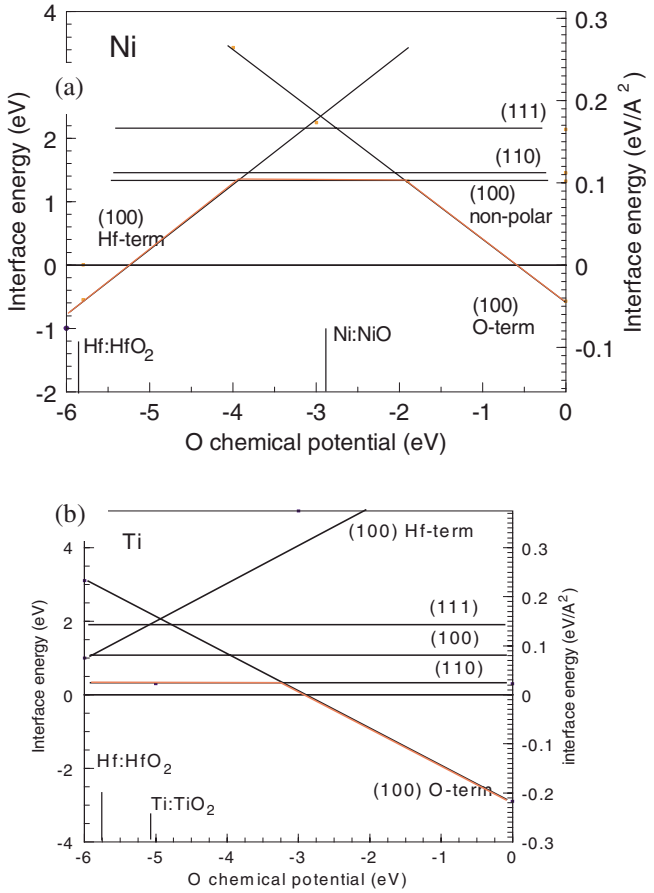

FIG. 8. (Color online) Interface formation energy vs oxygen chemical potential, for (a) Ni on HfO_2 and (b) Ti on HfO_2. Ni represents a high work function metal, Ti represents a low work function metal.

corresponding to the Hf:HfO_2 equilibrium. Also shown is the μ_0 of the Ni:NiO equilibrium, −2.9 eV.

The most stable interface at a given μ is shown by the red bold line. For the Ni:HfO_2 interface at μ=0, the O-terminated interface is most stable. Its interfacial energy increases as μ decreases, until a nonpolar interface becomes the most stable. Nonpolar interfaces have interface energy independent of μ, as they have no excess O. Figure 8(a) plots all three nonpolar interfaces. Interestingly, the stoichiometric (100) interface is slightly more stable than (110), when expressed as J/m^2 rather than eV per surface Ni, despite its structural vacancies. This is because of the higher atomic density of (100). The (110) interface is more stable than our (111) interface, they have similar density.

At even lower μ values, the Hf-terminated (100) becomes the most stable. Here the most stable configuration has sixfold bonded Hf sites, bonded to four oxygen and two Ni's.

We have created equivalent calculations for most transition metals on HfO_2. Figure 8(b) shows the equivalent diagram to Fig. 8(a) for a more electropositive, low work function metal, Ti. We see that O-terminated interface is stable over a much wider range of μ. The nonpolar interface is stable below a μ value intermediate between that of the Hf:HfO_2 and Ti:TiO_2 equilibrium. The (110) interface is more stable than the nonpolar (100) version. The metal-

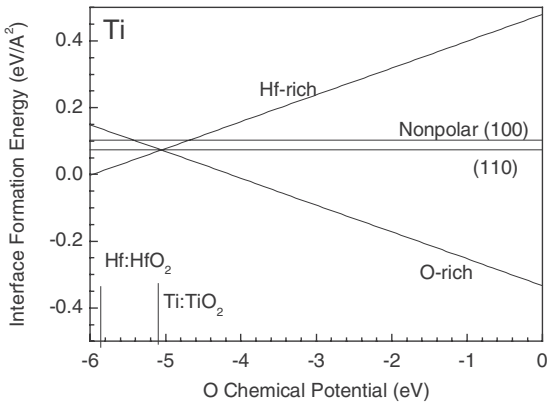

FIG. 9. Interface formation energy for bcc Ti on HfO_2 vs oxygen chemical potential,

terminated interface is never the most stable for accessible μ values.

We have calculated the equivalent interface energy diagrams for interfaces with the metals in a bcc phase, as in Fig. 9 Figure 10 shows this for the interfaces against large metals such as *Y*. The different behavior of electropositive and electronegative metals is the same as in Fig. 8. One key difference is that the slopes of formation energy vs. μ_O is now half that for Fig. 8, due to the lower metal atom density at the interface, q in Eq. (1). It is also interesting that for *Y* or La, the (111) interface is very stable in both nonpolar and polar forms.

In order to compare chemical trends, we now plot in Fig. 11(a) the interfacial energies for fcc polar, O terminated interfaces at $\mu_O=0$ and the nonpolar interfaces for each metal across the transition metal (TM) series. Figure 11(b) plots this against the experimental[66] metal work function value. Two broad trends are seen. The first is that the interface energy for O-rich (100) faces decreases from left to right across the TM series. This is because the interface M-O bond becomes less stable for the less electropositive metals with low work function at the right-hand end, as the M-O bond energy varies directly with the metal work function, Fig. 12. Note that this trend only continues to the Ni, Pd, and Pt column. After that, for Cu and Zn, the *d* band is filled and the metal work function falls. The second trend is that the interface energies of nonpolar interfaces are relatively constant across the series. This is because, as can be seen in Fig. 5(e), a nonpolar interface consists of both metal-metal (M-Me) and metal-oxygen (M-O) bonds, so that as M-O bonds become weaker, the M-Me bonds become slightly stronger, as noted by Shiraishi.[13] Note also that the trends are smoother against atomic number than against work function. This might be because the experimental work function values have small errors.

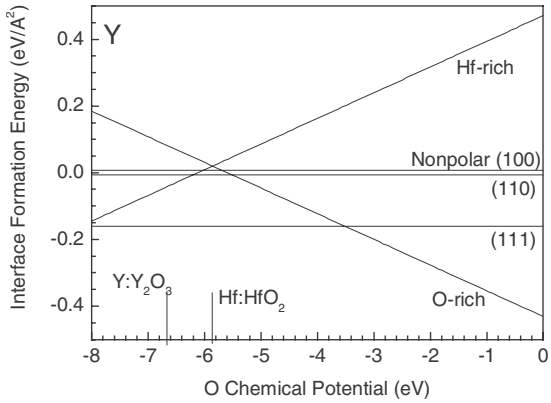

FIG. 10. Interface formation energy for "large cell" fcc *Y* on HfO_2 vs oxygen chemical potential.

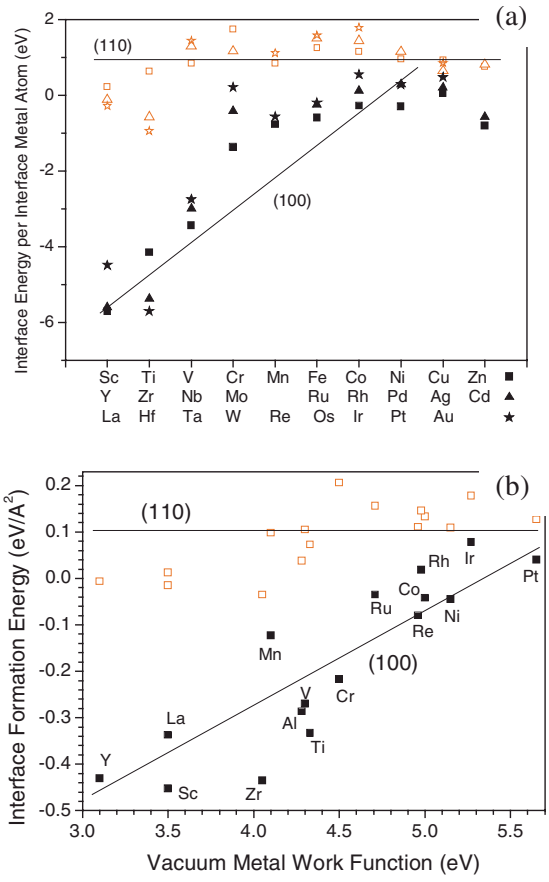

FIG. 11. (Color online) (a) Interface energy vs metal for each transition metal series and (b) vs metal work function. Note that the energy is roughly constant for nonpolar (110) interface, but strongly dependent on metal for polar (100).

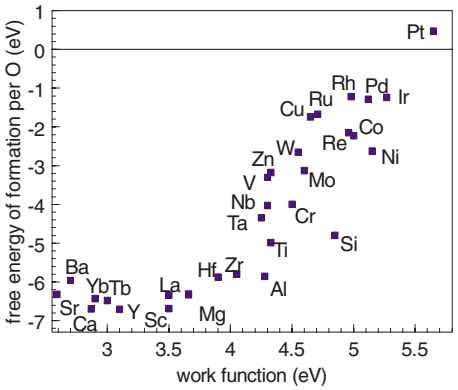

FIG. 12. (Color online) Free energy of formation of metal oxides, per O atom, vs metal work function.

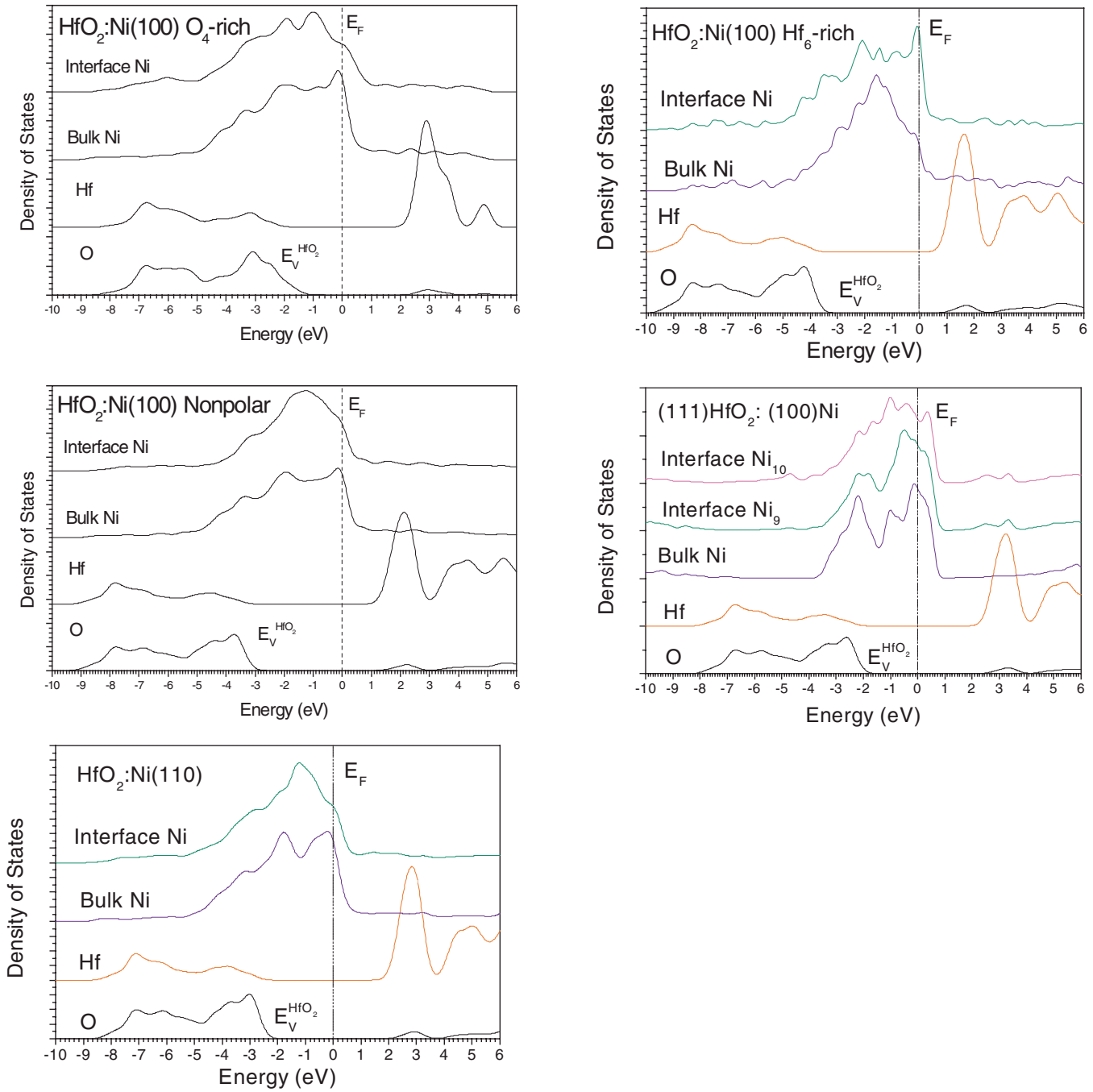

FIG. 13. (Color online) Local density of states for various Ni:HfO_2 interfaces from which valence-band offsets are extracted.

D. Barrier heights

The hole barrier heights (valence-band offsets) were calculated as the energy difference between the oxide valence-band edge and the metal Fermi energy for atoms in the center of the oxide and metal layers. Typical cases are shown for Ni on HfO_2 in Fig. 13. The band offset depends on the lattice strain of the oxide or metal. Thus, we corrected each band offset for the shift in going from the bulk phase to a strained bulk with the same lattice constants as in supercell.[17,59] The oxide valence-band edge is also shifted down by the 1.23 eV GW correction to the band gap.[59]

Figure 14(a) plots the valence-band offset (VBO) or hole barrier height across the 3*d* transition metal series. The VBO is seen to fall reasonably monotonically from Ti to Co and then rise again to Zn, for the nonpolar (110) interface. The trend is similar for the polar (100) interface except the VBO stays the same after Co.

Figure 14(b) plots the same VBO values against the vacuum work functions of the metals, including data from 4*d* and 5*d* metals. A number of points are seen. First, the slope of the VBO vs. work function is close to unity, in fact $S \sim 0.92$. This is much larger than the empirical MIGS estimate[5] of $S=0.5$. It means that the interface is essentially unpinned in explicit calculations, and that the EWF can easily scan the Si band gap. Second, there is a strong systematic difference between the O-terminated (100), nonpolar (110),

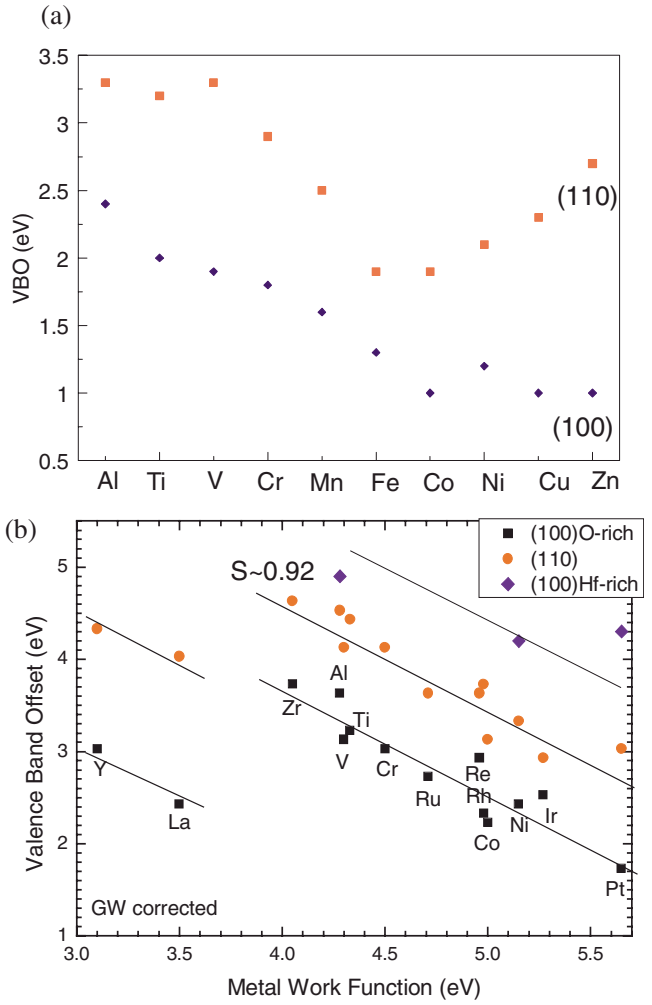

FIG. 14. (Color online) (a) Valence-band offset of metal-HfO_2 interfaces vs metal, across the first transition metal series. (b) Valence-band offset of metal-HfO_2 interfaces vs metal work function. Includes GW correction. The slope of the lines $S=0.92$.

and Hf-terminated (100) values, with (110) lying roughly 0.8 eV above O-terminated (100) and Hf-terminated (100) lying a further 0.8 eV above (110). Thus the oxide termination has a very strong effect on the VBO, above the size for the Si band gap. This is beyond a MIGS model. This occurs because the extra negatively charged oxygen ions at the O-terminated interface, together with their positively charged image, create an interface dipole, which raises the oxide bands with respect to the metal for O-terminated (100), lowering its VBO. The reverse effect occurs for Hf-terminated (100).

It should be noted though that the Fig. 14 VBO values for the Hf-terminated case are approximate. For this case, the metal Fermi levels are moving up toward the HfO_2 conduction-band edge, which of course is artificially low due to the LDA band-gap error. This effect "pins" E_F below the HfO_2 conduction band. The data points we do show are only possible by choosing pseudopotentials which give a larger than usual LDA band gap for HfO_2.

A third point is that there is considerable scatter in the trend of VBO vs work function. This was also found by Dong *et al.*[15] Interestingly, there is less scatter when plotted along the Period, in Fig. 14(a). It is often noted that the 4*d* series is simpler to analyze than the 3*d* series, because there is no ferromagnetism in the 4*d*'s.

TABLE II. Comparison of calculated and experimental valence-band offsets for metals on HfO_2

	Calculated VBO	Experimental VBO (eV)
Hf[a]	3.8 (nonpolar)	4.23
Ni[b,c]	3.4 (nonpolar)	3.32–2.6
Re[d]	3.5 (nonpolar)	4.2
RuOx[e]	2.7 (O rich)	3.05

[a]Reference 66.
[b]Reference 67.
[c]Reference 68.
[d]Reference 69.
[e]Reference 70.

The band offsets for the other nonpolar interfaces such as (110) follow the same trend as for nonpolar (100).

IV. DISCUSSION

The barrier height or VBO trends shown in Fig. 14 confirm that the abrupt, defect-free metal: HfO_2 interfaces form unpinned Schottky barriers with large S. A similar conclusion was found by Dong *et al.*[15] for interfaces on ZrO_2, for a much smaller range of metals. The trends are also similar to those found by Goniakowski and Noguera[53] for metal: MgO interfaces.

We can also compare the calculated VBOs with those measured experimentally by photoemission,[67–72] in Table II. There is reasonable agreement if the appropriate interface is compared.

The barrier height data of Fig. 14 for metal: HfO_2 interfaces can be compared to those for other systems. The ~0.9 eV difference in VBO between nonpolar and polar interfaces is due to the greater dipole at the polar interface. This difference is larger than seen in semiconductor interfaces, and it is due to the lower screening. The change in VBO can be expressed as

$$\Delta V = \frac{Nqd}{\varepsilon_\infty}, \tag{3}$$

where N is the interface dipole density, q is the charge, d is the dipole length and screening is provided by the electronic dielectric constant ε_∞. Typical VBO changes are 0.2 eV for Si or GaAs (for example the *A* and *B* interfaces of $Si:NiSi_2$ (Ref. 26) or those of GaAs)[30] where $\varepsilon=12$, $\Delta V \sim 0.9$ eV for HfO_2 with $\varepsilon_\infty=2.1$, and 3–4 eV for $Si:CaF_2$ interfaces[73] where $\varepsilon_\infty=1.2$. The same effect causes the large change in electron affinity of the between the clean and hydrogen-terminated diamond surface due to C-H surface dipoles.[74,75] There $\Delta V \sim 2.0$ eV, N is large, but q is small due to the small electronegativity difference of C and H, and ε is small.

Returning to the metal: HfO_2 system, the absence of strong pinning is an important conclusion for high K/metal

gate stacks in CMOS. It shows that it is possible in principle to choose metals with a wide enough range of effective work functions for nFETs and pFETs. This is also possible experimentally, in the more recent data of Wen *et al.*[8] We extracted a value of $S \sim 0.8$, by plotting the SBH data on HfO_2 against the barrier height on SiO_2.[76]

The absence of pinning at ideal interfaces indicates that extrinsic factors must be responsible for the observed pinning at real interfaces. Many of these effects occur for pFET metals,[11,12] which have a high work function. A model for this mechanism has been proposed by Akasaka *et al.*[18] and Robertson *et al.*[19] The basic mechanism is that high work function metals are also permeable to oxygen and hydrogen. Thus, the ambient can create oxygen vacancies in the high K oxide, by passing through the gate electrode. If this is stopped, the effect can be reduced. The effect also needs a reaction of the Si channel. The effect also requires oxygen diffusion, to allow oxygen vacancies to exist away from the gate electrode. This explains why more refractory gate electrode materials such as metal silicides and nitrides with low diffusion rates are useful, and why mixed oxides with lower oxygen diffusion rates show less pinning.

It is necessary to ask why MIGS do not cause the pinning predicted by the simple models.[5,6] In the analysis of Cowley and Sze,[20] the pinning factor S depends on the interface dipole $N\delta$ as

$$S = \frac{1}{1 + \dfrac{e^2 N\delta}{\varepsilon\varepsilon_0}} \tag{4}$$

where N is the areal density of MIGS and δ is the MIGS decay length into the oxide. MIGS have been observed by electron-energy-loss spectroscopy even in wide gap oxides such as MgO.[77] Demkov[14] calculated that the MIGS decay length δ is close to that expected from the scaling of δ with ε_∞.[23,24] The error must lie in the empirical formula used in the MIGS model,[23] to represent S in Eq. (4) or

$$S = \frac{1}{1 + 0.1(\varepsilon_\infty - 1)^2} \tag{5}$$

This has overestimated the MIGS density of states N. This formula (5) overestimates the pinning for wide gap oxides. Nevertheless the basic idea behind the MIGS model is correct, in the absence of defects.

Thus, the Fermi level pinning observed experimental is due to oxide defects. The mechanism for this is explained by Akasaka *et al.*[18] and Robertson *et al.*[19] A chemical reaction between the oxide, the metal gate and the Si allows the creation of oxygen vacancies at relative low cost, for metals of high work function. The vacancies become positively charged and cause band bending in the oxide which raises the metal gate Fermi level with respect to the Si channel band energy reference. The process is thermally activated, due to diffusion of oxygen across the oxide, consistent with the experimental situation.[11,12,78–80] A polar O-terminated interface can be converted into a nonpolar interface by diffusion O vacancies to the interface, where they annihilate at the extra oxygen atoms.[81]

V. CONCLUSIONS

The interface barrier heights of a wide range of metals on cubic HfO_2 have been calculated by *ab initio* methods for realistic atomic models for both polar and nonpolar interfaces. The stable interface geometries have fourfold coordinated oxygen. The valence-band offsets or barrier heights are found to depend strongly on the metal work function, consistent with a Schottky barrier pinning factor S of about 0.92. This dependence is much stronger than in the MIGS model. There is a large interface dipole for polar O-rich interfaces, which reduces their hole barrier heights by about 0.8 eV below that of nonpolar interfaces. Overall, the results show little intrinsic Schottky barrier pinning. The experimentally observed pinning in must be due to an extrinsic mechanism such as band bending due to charged oxygen vacancies.

[1] B. H. Lee, J. Oh, H. H. Tseng, R. Jammy, and H. Huff, Mater. Today **9**, 32 (2006).
[2] E. P. Gusev, V. Narayanan, and M. M. Frank, IBM J. Res. Dev. **50**, 387 (2006).
[3] J. Robertson, Rep. Prog. Phys. **69**, 327 (2006).
[4] D. G. Schlom and J. H. Haeni, MRS Bull. **27**, 198 (2002).
[5] J. Robertson, J. Vac. Sci. Technol. B **18**, 1785 (2000); J. Non-Cryst. Solids **303**, 94 (2002); P. W. Peacock and J. Robertson, J. Appl. Phys. **92**, 4712 (2002).
[6] Y. C. Yeo, T. J. King, and C. Hu, J. Appl. Phys. **92**, 7266 (2002).
[7] J. K. Schaeffer *et al.*, *Tech Digest IEDM* (IEEE, New York, 2004), p. 287.
[8] H. C. Wen, P. Majhi, K. Choi, C. S. Park, H. N. Alshareef, H. R. Harris, H. Luan, H. Miimi, H. B. Park, G. Bersuker, P. S. Lysaght, D. L. Kwong, S. C. Song, B. H. Lee, and R. Jammy, Microelectron. Eng. **85**, 2 (2008).
[9] K. Mistry, P. Packan, *et al.*, *Tech Digest IEDM* (IEEE, New York, 2007), pp. 28.4.
[10] V. Narayanan, V. K. Paruchuri, N. A. Bojarczuk, B. P. Linder, B. Doris, Y. H. Kim, S. Zafar, J. Stathis, S. Brown, J. Arnold, M. Copel, E. Cartier, A. Callegari, S. Guha, G. Shahidi, and T. C. Chen, Symposium on VLSI Technology Digest of Technical Papers (IEEE, New York, 2006), p. 24.
[11] J. K. Schaeffer, L. R. C. Fonseca, S. B. Samavedam, Y. Liang, P. J. Tobin, and B. E. White, Appl. Phys. Lett. **85**, 1826 (2004).
[12] E. Cartier, F. R. McFeely, V. Narayanan, P. Jamison, M. Copel, and G. Shahidi, *Symposium on VLSI Technology Digest* (IEEE, New York, 2005), p. 15.
[13] K. Shiraishi *et al.*, *Tech Digest IEDM* (IEEE, New York, 2005), p. 43.
[14] A. A. Demkov, Phys. Rev. B **74**, 085310 (2006).
[15] Y. F. Dong, S. J. Wang, Y. P. Feng, and A. C. H. Huan, Phys. Rev. B **73**, 045302 (2006).
[16] A. A. Knizhnik, I. M. Iskandarov, A. A. Bagaturyants, B. V.

Potapkin, and L. R. C. Fonseca, J. Appl. Phys. **97**, 064911 (2005).
[17] K. Y. Tse and J. Robertson, Phys. Rev. Lett. **99**, 086805 (2007).
[18] Y. Akasaka, G. Nakamura, K. Shiraishi, N. Umezawa, K. Yamabe, O. Ogawa, and K. Nakamura, Jpn. J. Appl. Phys. **45**, L1289 (2006).
[19] J. Robertson, O. Sharia, and A. A. Demkov, Appl. Phys. Lett. **91**, 132912 (2007).
[20] A. W. Cowley and S. M. Sze, J. Appl. Phys. **36**, 3212 (1965).
[21] J. Tersoff, Phys. Rev. Lett. **52**, 465 (1984).
[22] W. Mönch, Phys. Rev. Lett. **58**, 1260 (1987).
[23] W. Mönch, Surf. Sci. **299-300**, 928 (1994).
[24] W. Mönch, Appl. Surf. Sci. **92**, 367 (1996).
[25] R. T. Tung, Phys. Rev. Lett. **84**, 6078 (2000).
[26] G. P. Das, P. Blochl, O. K. Andersen, N. E. Christensen, and O. Gunnarsson, Phys. Rev. Lett. **63**, 1168 (1989).
[27] A. Ruini, R. Resta, and S. Baroni, Phys. Rev. B **56**, 14921 (1997).
[28] J. Bardi, N. Binggeli, and A. Baldereschi, Phys. Rev. B **59**, 8054 (1999).
[29] M. Peressi, N. Binggeli, and A. Baldereschi, J. Phys. D **31**, 1273 (1998).
[30] M. Peressi, S. Baroni, R. Resta, and A. Baldereschi, Phys. Rev. B **43**, 7347 (1991).
[31] C. Berthod, N. Binggeli, and A. Baldereschi, Phys. Rev. B **68**, 085323 (2003).
[32] M. Nunez and M. Buongiorno Nardelli, Phys. Rev. B **73**, 235422 (2006).
[33] U. Diebold, J. M. Pan, and T. E. Madey, Surf. Sci. **331-333**, 845 (1995).
[34] H. J. Freund, H. Kuhlenbeck, and V. Staemmler, Rep. Prog. Phys. **59**, 283 (1996).
[35] G. Pacchioni, L. Giordano, and M. Baistrocchi, Phys. Rev. Lett. **94**, 226104 (2005).
[36] Q. Fu and T. Wagner, Surf. Sci. Rep. **62**, 431 (2007).
[37] H. J. Freund, Surf. Sci. **601**, 1438 (2007).
[38] A. M. Stoneham and P. W. Tasker, J. Phys. C **18**, L543 (1985).
[39] M. W. Finnis, Surf. Sci. **241**, 61 (1991).
[40] M. W. Finnis, Acta Metall. **40**, S25 (1992).
[41] D. M. Duffy, J. H. Harding, and A. M. Stoneham, Acta Metall. **40**, S11 (1992).
[42] U. Schonberger, O. K. Andersen, and M. Fethfessl, Acta Metall. **40**, S1 (1992).
[43] C. Kruse, M. W. Finnis, J. S. Lin, M. C. Payne, and V. Y. Milman, Philos. Mag. Lett. **73**, 377 (1996).
[44] I. G. Batirev, A. Alavi, M. W. Finnis, and T. Deutsch, Phys. Rev. Lett. **82**, 1510 (1999).
[45] C. Verdozzi, D. R. Jennison, P. A. Schultz, and M. P. Sears, Phys. Rev. Lett. **82**, 799 (1999).
[46] A. Bogicevic and D. R. Jennison, Phys. Rev. Lett. **82**, 4050 (1999).
[47] W. Zhang, J. R. Smith, and A. G. Evans, Acta Mater. **50**, 3803 (2002).
[48] X. G. Wang, J. R. Smith, and A. G. Evans, Phys. Rev. B **74**, 081403(R) (2006).
[49] D. J. Siegel, L. G. Hector, and J. B. Adams, Phys. Rev. B **65**, 085415 (2002).
[50] X. G. Wang, A. Chaka, and M. Scheffler, Phys. Rev. Lett. **84**, 3650 (2000).
[51] M. W. Finnis, J. Phys.: Condens. Matter **8**, 5811 (1996).
[52] J. Goniakowski and C. Noguera, Phys. Rev. B **66**, 085417 (2002).
[53] J. Goniakowski and C. Noguera, Interface Sci. **12**, 93 (2004).
[54] J. I. Beltran, S. Gallego, J. Cerda, J. S. Moya, and M. C. Munoz, Phys. Rev. B **68**, 075401 (2003).
[55] M. C. Munoz, S. Gallego, J. I. Beltran, and J. Cerda, Surf. Sci. Rep. **61**, 303 (2006).
[56] M. Mrovec, J. M. Albina, B. Meyer, and C. Elsasser, Phys. Rev. B **79**, 245121 (2009).
[57] D. G. Pettifor, Solid State Phys. **40**, 43 (1987); V. L. Moruzzi, A. R. Williams, and J. F. Janak, Phys. Rev. B **15**, 2854 (1977).
[58] M. D. Segall, P. Lindan, M. J. Probert, C. J. Pickard, P. J. Hasnip, S. J. Clark, and M. C. Payne, J. Phys.: Condens. Matter **14**, 2717 (2002).
[59] V. Fiorentini and G. Gulleri, Phys. Rev. Lett. **89**, 266101 (2002).
[60] B. Kralik, E. K. Chang, and S. G. Louie, Phys. Rev. B **57**, 7027 (1998).
[61] P. W. Tasker, J. Phys. C **12**, 4977 (1979).
[62] C. Noguera, J. Phys.: Condens. Matter **12**, R367 (2000); J. Goniakowski, F. Finocchi, and C. Noguera, Rep. Prog. Phys. **71**, 016501 (2008).
[63] W. A. Harrison, E. A. Kraut, J. R. Waldrop, and R. W. Grant, Phys. Rev. B **18**, 4402 (1978).
[64] P. W. Peacock and J. Robertson, Phys. Rev. Lett. **92**, 057601 (2004).
[65] A. Christensen and E. A. Carter, J. Chem. Phys. **114**, 5816 (2001).
[66] H. B. Michaelson, J. Appl. Phys. **48**, 4729 (1977).
[67] S. Suzer, S. Sayan, M. M. Banaszak Holl, E. Garfunkel, Z. Hussain, and N. M. Hamdan, J. Vac. Sci. Technol. A **21**, 106 (2003).
[68] Y. F. Dong, S. J. Wang, J. W. Chai, Y. P. Feng, and A. C. H. Huan, Appl. Phys. Lett. **86**, 132103 (2005).
[69] Q. Li, Y. F. Dong, S. J. Wang, J. W. Chai, A. C. H. Huan, Y. P. Feng, and C. K. Ong, Appl. Phys. Lett. **88**, 222102 (2006).
[70] Y. Liang, J. Curless, C. J. Tracy, D. C. Gilmer, J. K. Schaeffer, D. H. Triyoso, and P. J. Tobin, Appl. Phys. Lett. **88**, 072907 (2006).
[71] D. Lim, R. Haight, M. Copel, and E. Cartier, Appl. Phys. Lett. **87**, 072902 (2005).
[72] Q. Li, S. J. Wang, K. B. Li, A. C. H. Huan, J. W. Chai, J. S. Pan, and C. K. Ong, Appl. Phys. Lett. **85**, 6155 (2004).
[73] S. Satpathy and R. M. Martin, Phys. Rev. B **39**, 8494 (1989).
[74] J. B. Cui, J. Ristein, and L. Ley, Phys. Rev. Lett. **81**, 429 (1998).
[75] M. J. Rutter and J. Robertson, Phys. Rev. B **57**, 9241 (1998).
[76] J. Robertson, J. Vac. Sci. Technol. B **27**, 277 (2009).
[77] D. A. Muller, D. A. Shashkov, R. Benedek, L. H. Yang, J. Silcox, and D. N. Seidman, Phys. Rev. Lett. **80**, 4741 (1998).
[78] S. C. Song, C. S. Park, J. Price, R. Choi, H. H. Tseng, B. H. Lee, and R. Jammy, *Tech Digest IEDM* (IEEE, New York, 2007), p. 13.3.
[79] K. Akiyama, W. Wang, W. Mizubayashi, M. Ikeda, H. Ota, T. Nabatame, and A. Toriumi, *Tech Digest VLSI* (IEEE, New York, 2008), p. 8.3.
[80] J. Schaeffer, D. C. Gilmer, S. Samevadam, M. Raymond, A. Haggag, S. Kalpat, B. Seimie, C. Capasso, and B. E. White, J. Appl. Phys. **102**, 074511 (2007).
[81] O. Sharia, K. Tse, J. Robertson, and A. A. Demkov, Phys. Rev. B **79**, 125305 (2009).